12th International Symposium on Turbulence and Shear Flow Phenomena (TSFP12)
Osaka, Japan (Online), July 19-22, 2022

SCALING OF ROUGH-WALL TURBULENCE IN A TRANSITIONALLY ROUGH REGIME

Guo-Zhen Ma
Department of Engineering Mechanics
Tsinghua University
Haidian District, Beijing, 100084, P. R. China
mgz17@mails.tsinghua.edu.cn

Chun-Xiao Xu
Department of Engineering Mechanics
Tsinghua University
Haidian District, Beijing, 100084, P. R. China
xucx@tsinghua.edu.cn

Hyung Jin Sung
Department of Mechanical Engineering
KAIST
Daejeon 34141, Republic of Korea
hjsung@kaist.ac.kr

Wei-Xi Huang
Department of Engineering Mechanics
Tsinghua University
Haidian District, Beijing, 100084, P. R. China
hwx@tsinghua.edu.cn

ABSTRACT

Direct numerical simulations (DNSs) were performed for a turbulent channel flow over three-dimensional sinusoidal rough walls to test a roughness scaling method in a transitionally rough regime. Three groups of rough cases were employed to assess the scaling formula by systematically varying the friction Reynolds number Re_τ and the ratio of the roughness height k to the channel half-height δ, and their predictions were compared with Nikuradse's experimental data and other roughness types. A new coupling scale $Re_\tau/(\bar{k}^+S)^n$ is then proposed by combining Re_τ and in a logarithmic form, where n is the scaling exponent, $\bar{k}^+$ is the viscous-scaled mean roughness height and S is the roughness steepness. All the simulated data for the roughness function and the peak of the streamwise turbulent velocity fluctuations collapse into single curves with this coupling scale. Our investigation of the rough-wall scaling behavior with DNS data can serve as a basis for supplementing Moody's data in the transitionally rough regime.

INTRODUCTION

Turbulent flow over a rough wall almost always produces higher drag than that of a smooth wall. The increase in drag is often quantified by the roughness function ΔU^+, which reflects the downward shift of the mean velocity profile (Hama, 1954). In practice, the increase of drag usually brings a lot of harm and efficiency loss, and predicting the drag on a rough wall is therefore of crucial importance to most engineering problems. A central goal in the present study is to predict the roughness function directly from the given rough surface and flow conditions, and then predict the wall resistance.

The dependences of the roughness function on the roughness height and other geometric features such as the roughness density and shape have been explored extensively for various types of roughness (Chung *et al.*, 2021). Some scales for the equivalent sand grain roughness have been found (Flack & Schultz, 2010). However, the influence of the Reynolds number is usually not considered in these scaling methods. Furthermore, the Reynolds-number scaling of the second-order statistics has to the best of our knowledge not been reported in the literature for rough-wall turbulence. In the present study, the Reynolds number and the wall roughness parameters are comprehensively considered, to parameterize the turbulent statistics.

NUMERICAL SIMULATION

The problem under consideration is the fully developed turbulent channel flow over three-dimensional sinusoidal rough walls. A schematic diagram of the channel is shown in figure 1. A right-handed Cartesian frame fixed in the physical space is employed with x, y and z axes along the streamwise, vertical and spanwise coordinates, respectively. The corresponding velocity components in the three directions are u, v and w. The flow is driven by a mean pressure gradient, which is dynamically adjusted to keep the constant flow rate in time. For the roughness parameters, k is the semi-amplitude of the sinusoidal roughness and λ is the wavelength of the roughness elements. The governing equations are the dimensionless incompressible Navier-Stokes and continuity equations:

$$\begin{cases} \dfrac{\partial \mathbf{u}}{\partial t} + \mathbf{u}\cdot\nabla\mathbf{u} = -\nabla p + \dfrac{1}{Re_b}\nabla^2\mathbf{u} \\ \nabla\cdot\mathbf{u} = 0 \end{cases} \tag{1}$$

where $\mathbf{u} = (u, v, w)$ are the velocity components, p is the pressure and Re_b is the bulk Reynolds number. The above equations are discretized by using a pseudo-spectral method in the x- and z-directions and a second-order finite-difference scheme on the staggered grids in the y-direction. A third-order time-splitting method is employed for time advancement. To deal with the deformation boundary, we use a coordinate transformation to transform the irregular physical domain (x, y, z) into a rectangular computational domain (ξ_1, ξ_2, ξ_3) based on the boundary-fitted system. The periodic condition is applied in the streamwise and spanwise directions, and the no-slip condition is applied to the walls of the channel. More details regarding the numerical methods and analysis procedures can be found in Zhang *et al.* (2019).

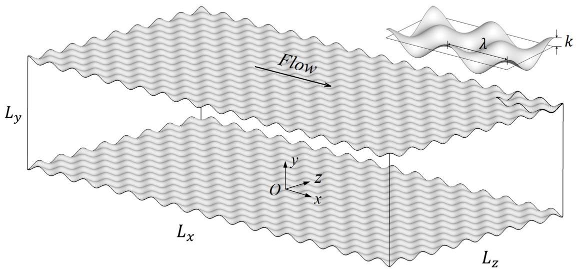

Figure 1. Schematic diagram of the turbulent channel flow over three-dimensional sinusoidal rough walls.

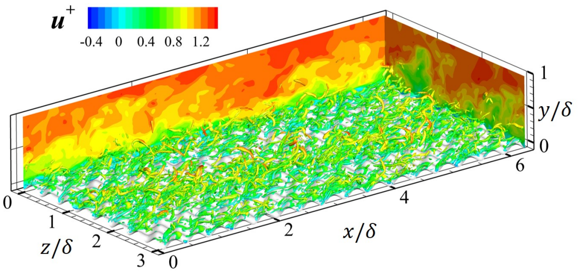

Figure 2. Instantaneous vortical structures over rough walls. Contours of the instantaneous streamwise velocity are plotted in the $x-y$ plane and the $y-z$ plane.

In this work, three groups of numerical cases were simulated with reference to Nikuradse's pipe experiment: (1) $k/\delta = 1/18$; (2) $k/\delta = 1/54$; (3) $k/\delta = 1/108$. For each group, the friction Reynolds number was systematically varied in the range 180 to 1080, while the physical geometrical size of the roughness element relative to the half-channel height was kept constant. The size of the computational domain is $2\pi\delta \times 2\delta \times \pi\delta$ for the all cases, where δ is the half channel height. The mesh is uniformly spaced in the streamwise and spanwise directions, and stretched in the wall-normal direction according to a cosine distribution. A detailed list of the roughness parameters and computational parameters can be found in Table 1.

RESULTS

Figure 2 shows the instantaneous three-dimensional vortical structures, to visually describe the differences in turbulent flow field caused by roughness elements. Here, we take the rough case $k^+ = 30$, $\lambda^+ = 212$ at $Re_\tau = 540$ of as an example. The overlying vortical structures are visualised via the isosurface of the local swirling strength λ_{ci}. The vortical structures of the rough cases are dense and finely fragmented vortical structures appear near the roughness elements as compared with the smooth-wall case. The streamwise size, inclination angle and distribution pattern of these vortices are modulated by the rough form and rough parameters (De Marchis *et al.*, 2015). Note that the low-speed zones are lifted up in the *y*-*z* plane, corresponding to the formation of the streaky structures. To study more quantitatively the effects of roughness, turbulent statistics are presented and discussed in the following.

The increase in wall drag caused by the surface roughness is manifested in the streamwise mean velocity profile as a downward shift in the logarithmic region, known as the roughness function ΔU^+, as shown in figure 3. The roughness function is itself a function of the roughness Reynolds number. The

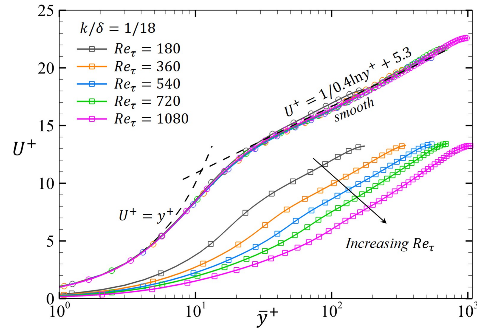

Figure 3. Profiles of the mean streamwise velocity for $k/\delta = 1/18$. The circle symbols represents smooth-wall cases, the square symbols represent the rough-wall cases, and the colors represent different Reynolds numbers.

logarithmic law for a smooth wall and a rough wall respectively can be expressed as

$$U_r^+ = \frac{1}{\kappa}\ln y^+ + C - \Delta U^+, \tag{2}$$

where κ is the von Kármán constant and C is the offset constant, here $\kappa = 0.40$ and $C = 5.3$. The velocity profiles decrease significantly with the increase of Reynolds number, that is, and the main factor affecting the roughness function is the roughness height k^+. In our previous study (Ma *et al.*, 2020), we found that the roughness function is strongly correlated with the proportion of wall pressure drag and total drag, while the roughness height has a significant impact on the pressure drag. In addition, the mean velocity profiles of three groups of rough cases all satisfy the log law from a certain position above the crest of the roughness elements. Therefore, from the perspective of first-order statistics, the hypothesis of outer-layer similarity is still satisfied for rough-wall cases (Townsend, 1976). For the other two groups of cases, the variation trend is similar to that of $k^+ = 1/18$.

The presence of roughness elements has a significant effect on the velocity fluctuations. According to the phase average and triple decomposition, the second-order velocity correlation can be decomposed into three parts, i.e.

$$\overline{u_i u_j} == \overline{u}_i \overline{u}_j + \overline{\tilde{u}_i \tilde{u}_j} + \overline{u_i' u_j'}, \tag{3}$$

where the second and third terms on the right-hand side denote the dispersive and Reynolds stresses, which correspond to the wave-induced and turbulent components, respectively. Figure 4 shows the streamwise Reynolds stress profiles with respect to the wall-normal height for $k/\delta = 1/18$. Compared with the smooth-wall case, the roughness elevates the wall-normal location about a roughness height, and the peak intensity of the Reynolds stresses decreases with increasing k^+, which indicates that the typical coherent structures near the wall are disrupted, and the turbulent fluctuations are weakened. The larger roughness viscous scale causes more significant suppression of the near-wall turbulence. In the outer region, the profiles collapse with the smooth-wall case at higher vertical positions, supporting the Townsend's outer-layer similarity hypothesis.

Further, figure 5 shows the streamwise dispersive stress profiles with respect to the wall-normal height for $k/\delta = 1/18$. For the smooth-wall case, $\overline{\tilde{u}\tilde{u}}^+$ should be zero. The profiles

Table 1. Reynolds number, roughness parameters and computational setup. Δx^+ and Δz^+ characterize the grid resolution in the streamwise and spanwise directions, respectively; Δy^+_{min} and Δy^+_c are the minimum grid resolution near the bottom boundary and the maximum grid resolution near the channel centerline in the vertical direction, respectively.

Case	Re_τ	k^+	λ^+	N_x, N_y, N_z	$\Delta x^+, \Delta y^+_{min}, \Delta y^+_c, \Delta z^+$
	180	10	71	144, 144, 144	7.85, 0.04, 4.0, 3.9
	360	20	141	192, 144, 192	11.78, 0.08, 7.9, 5.9
$k/\delta = 1/18$	540	30	212	288, 192, 288	11.78, 0.07, 7.9, 5.9
	720	40	283	384, 288, 384	11.78, 0.04, 7.9, 5.9
	1080	60	424	576, 384, 576	11.78, 0.04, 8.9, 5.9
	180	3.33	24	384, 288, 384	2.94, 0.01, 1.9, 1.47
	360	6.67	47	384, 288, 384	5.89, 0.02, 3.9, 2.9
$k/\delta = 1/54$	540	10	71	384, 288, 384	8.83, 0.03, 5.9, 4.4
	720	13.33	94	384, 288, 384	11.78, 0.04, 7.9, 5.9
	1080	20	141	576, 384, 576	11.78, 0.06, 8.9, 5.9
	180	1.67	12	576, 384, 576	1.96, 0.01, 1.5, 1.0
	360	3.33	24	576, 384, 576	3.93, 0.01, 2.9, 2.0
$k/\delta = 1/108$	540	5	35	576, 384, 576	5.89, 0.02, 4.4, 2.9
	720	6.67	47	576, 384, 576	7.85, 0.02, 5.9, 3.9
	1080	10	71	576, 384, 576	11.78, 0.04, 8.9, 5.9

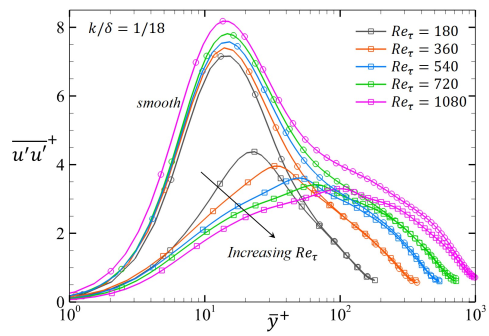

Figure 4. Profiles of the streamwise Reynolds stress for $k/\delta = 1/18$. The definitions of the lines and symbols are the same as those in Figure 2.

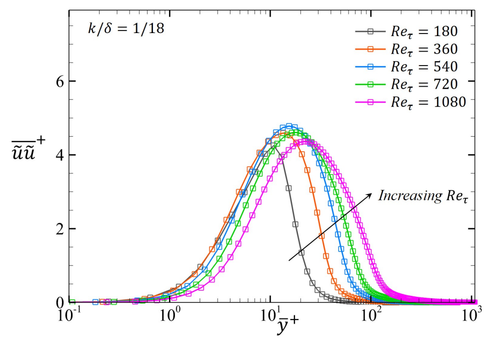

Figure 5. Profiles of the streamwise dispersive stress for $k/\delta = 1/18$. The definitions of the lines and symbols are the same as those in Figure 2.

show an outward shift as the roughness Reynolds number k^+ increases, but do not show a monotonic variation different from the Reynolds stress profiles. This may be related to the ξ_2-plane average method (Zhang *et al.*, 2019). Even so, the dispersive stresses for all the cases are dominant within the roughness sublayer but drop rapidly to zero above the crest of roughness elements.

According to the above analysis, it's known that the mean velocity profiles and Reynolds stress profiles in the rough-wall turbulence are affected by both the Reynolds number and the roughness height. While our previous study (Ma *et al.*, 2020) showed that the coupling scale k^+S produces a more reliable prediction than the equivalent sand grain roughness height k_s^+ for various types of roughness, where S is the roughness steepness, i.e. the absolute streamwise gradient of the surface. Therefore, we first consider the scaling relationship between the roughness function and the Reynolds number and the roughness height. The roughness function $\Delta\bar{U}^+$ is calculated by the mean bulk velocity $U^+_{b,s} - U^+_{b,r}$. Then $\Delta\bar{U}^+$ is plotted against $\bar{k}^+S$ in figure 6. All the data collapse onto a single line, i.e.

$$\Delta\bar{U}^+ = \frac{1}{\kappa}\ln\left(\bar{k}^+S\right)^{1.2} + 5.8, \tag{4}$$

where $\bar{k}^+$ is the arithmetic average of the absolute values of the profile height (Chan *et al.*, 2015). The goodness-of-fit R^2 is close to 0.97 for the above fitting function equation. Eq.(4) shows that the roughness function is only affected by the viscous-scaled roughness height k^+ and the rough shape parameter, i.e. the roughness steepness S, independent of the Reynolds number. In addition, some published data are

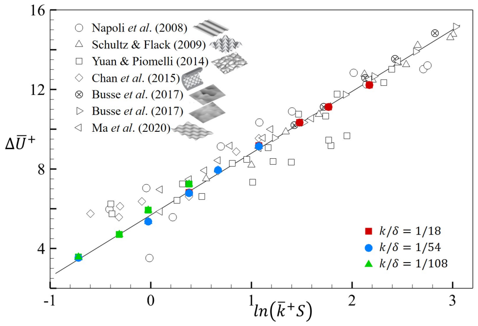

Figure 6. Variations of the roughness function $\Delta\bar{U}^+$ with the coupling roughness scale $\bar{k}^+S$.

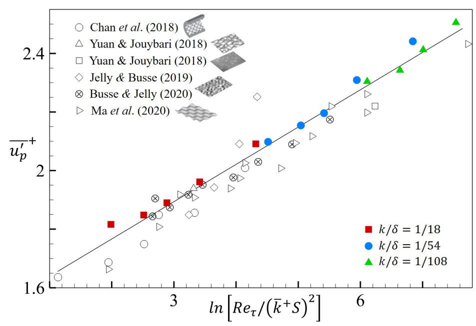

Figure 7. Variations of the roughness function $\overline{u'_p}^+$ with the coupling roughness scale $Re_\tau/(\bar{k}^+S)^2$.

added for comparison. Correspondingly, several roughness forms were chosen: the irregular random two-dimensional sinusoidal roughness (Napoli *et al.*, 2008), close-packed right-angle pyramids (Schultz & Flack, 2009), randomly rotated ellipsoid (Yuan & Piomelli, 2014), three-dimensional 'egg-carton' rough pipe (Chan *et al.*, 2015) and graphite and grit-blasted roughness. Good agreement with Eq.(4) is evident in all cases, which indicates that the relationship for wall resistance prediction is also valid for other roughness forms. However, different roughness forms bring forth different intercepts in the scaling formula Eq.(4) (Ma *et al.*, 2020), especially for random roughness patterns, which can be found in the literature (Ma *et al.*, 2022).

In smooth-wall turbulence, the peak intensity of the streamwise velocity fluctuations increases with the increase of Reynolds numbers (Marusic *et al.*, 2010). In order to comprehensively consider the effect of Reynolds number and wall roughness, we refer to the above scaling method applied to the roughness function and make a log-linear fit for $\overline{u'_p}^+$ as a function of $\bar{k}^+S$ and Re_τ as follows,

$$\overline{u'_p}^+ = 0.13\ln\left[\frac{Re_\tau}{(\bar{k}^+S)^2}\right] + 1.5. \tag{5}$$

An effective collapse of data onto a single curve is obtained, and the goodness-of-fit R^2 reaches 0.97. Figure 7 shows this scaling relationship, together with some published data (Chan *et al.*, 2018; Yuan & Jouybari, 2018; Jelly & Busse, 2019; Busse & Jelly, 2020; Ma *et al.*, 2020). Good agreement with Eq. (5) can be seen in all the data, indicating that $\overline{u'_p}^+$ for all these rough surfaces, both regular and random, two-dimensional and three-dimensional, scales with $Re_\tau/(\bar{k}^+S)^2$. Note that there is no variation in the intercepts in the scaling formula Eq.(5) for different roughness types, different from the roughness function. This arises the turbulent fluctuations presented here give all the turbulent components after triple decomposition, by which the influence of the unevenness of the spatial geometry due to roughness is isolated. Our results show that the streamwise turbulence fluctuation intensity has a strong correlation with the roughness function, which provides an alternative to k_s^+ as a means of characterizing rough walls.

CONCLUSIONS

In the present study, DNSs with a body-conforming grid were performed for turbulent channel flow over three-dimensional sinusoidal rough walls. With reference to Nikuradse's pipe experimental data, three groups of rough cases are considered by systematically varying the relative roughness height k/δ and the friction Reynolds number Re_τ. Our current simulations, which are mostly in the transitionally rough regime in term of the Moody's chart, where the turbulence statistics are both dependent on the Reynolds number and the roughness height. To this end, we proposed the combination of Re_τ and $\bar{k}^+$, i.e. $Re_\tau/(\bar{k}^+S)^n$, consistent with the theoretical derivation through a linear–log fit. Good data collapse is obtained. While compared with the equivalent sand grain roughness height k_s^+, $\bar{k}^+S$ appears to be the more suitable parameter, and indeed achieves a good scaling behaviour in the roughness function and the peak of the streamwise turbulent velocity fluctuations for various types of roughness forms. The present work can serve as a basis for substituting the widely-used Moody chart in engineering.

ACKNOWLEDGEMENTS

The authors acknowledge funding support from the National Natural Science Foundation of China under grant numbers 11772172 and 91752205 and the National Research Foundation of Korea (No. 2020R1A2C2008106).

REFERENCES

Busse, A. & Jelly, T. O. 2020 Influence of surface anisotropy on turbulent flow over irregular roughness. *Flow Turbul. Combust.* **104** (2), 331–354.

Chan, L., MacDonald, M., Chung, D., Hutchins, N. & Ooi, A. 2015 A systematic investigation of roughness height and wavelength in turbulent pipe flow in the transitionally rough regime. *J. Fluid Mech.* **771**, 743–777.

Chan, L., MacDonald, M., Chung, D., Hutchins, N. & Ooi, A. 2018 Secondary motion in turbulent pipe flow with three-dimensional roughness. *J. Fluid Mech.* **854**, 5–33.

Chung, D., Hutchins, N., Schultz, M. P. & Flack, K. A. 2021 Predicting the drag of rough surfaces. *Annu. Rev. Fluid Mech.* **53**, 439–471.

De Marchis, M., Milici, B. & Napoli, E. 2015 Numerical observations of turbulence structure modification in channel flow over 2d and 3d rough walls. *Intl J. Heat Fluid Flow* **56**, 108–123.

Flack, K. A. & Schultz, M. P. 2010 Review of hydraulic roughness scales in the fully rough regime. *J. Fluids Eng.* **132** (4), 041203.

Hama, F. R. 1954 Boundary layer characteristics for smooth and rough surfaces. *Trans. Soc. Nav. Archit. Mar. Engrs* **62**, 333–358.

Jelly, T. O. & Busse, A. 2019 Reynolds number dependence of reynolds and dispersive stresses in turbulent channel flow past irregular near-gaussian roughness. *Intl J. Heat Fluid Flow* **80**, 108485.

Ma, G. Z., Xu, C. X., Sung, H. J. & Huang, W. X. 2020 Scaling of rough-wall turbulence by the roughness height and steepness. *J. Fluid Mech.* **900**, R7.

Ma, G. Z., Xu, C. X., Sung, H. J. & Huang, W. X. 2022 Scaling of rough-wall turbulence in a transitionally rough regime. *Phys. Fluids* **34** (3), 031701.

Marusic, I., Mathis, R. & Hutchins, N. 2010 High reynolds number effects in wall turbulence. *Intl J. Heat Fluid Flow* **31** (3), 418–428.

Napoli, E., Armenio, V. & De Marchis, M. 2008 The effect of the slope of irregularly distributed roughness elements on turbulent wall-bounded flows. *J. Fluid Mech.* **613**, 385–394.

Schultz, M. P. & Flack, K. A. 2009 Turbulent boundary layers on a systematically varied rough wall. *Phys. Fluids* **21** (1), 015104.

Townsend, A A 1976 *The structure of turbulent shear flow*, 2nd edn. UK: Cambridge university.

Yuan, J & Jouybari, M Aghaei 2018 Topographical effects of roughness on turbulence statistics in roughness sublayer. *Phys. Rev. Fluids* **3** (11), 114603.

Yuan, J. & Piomelli, U. 2014 Estimation and prediction of the roughness function on realistic surfaces. *J. Turbul.* **15** (6), 350–365.

Zhang, W. Y., Huang, W. X. & Xu, C. X. 2019 Very large-scale motions in turbulent flows over streamwise traveling wavy boundaries. *Phys. Rev. Fluids* **4** (5), 054601.